Discovery of Late Triassic volcanic ash layers in the deep-water zone of the Nanpanjiang Basin (South China) and the possibility of Carnian Pluvial Episode correlation

Liangjun Wu^{a,b,c*}

- a. Institute of Karst Geology CAGS/Key Laboratory of Karst Dynamics, MNR & GZAR/International Research Centre on Karst under the Auspices of UNESCO, 541004, Guilin, China
- b. Pingguo Guangxi, Karst Ecosystem, National Observation and Research Station, 531406, Pingguo, China
- c. College of Earth Sciences, Jilin University, 130061, Changchun, China

The Nanpanjiang Basin is a major basin on the eastern margin of the Tethys Ocean (Fig. 1a). The Late Triassic was an important transition period for the Nanpanjiang Basin changing from marine to continental facies. The shift in the South China region from an extensional platform-basin environment to a foreland basin environment may have occurred during this period (Sun et al., 2016). Simultaneously, climates abrupt change from arid to humid occurred in the Late Triassic (Simms and Ruffell, 1989), known as the Carnian Pluvial Episode (CPE). This event caused an interruption in carbonate sedimentation in global marine platform facies regions, and areas around the Tethys Ocean generally transitioned to fluvial-deltaic sedimentation, such as the Formation of the largest delta system to date in the Boreal Ocean (Klausen and Nyberg, 2019).

Previous research on the CPE in the Nanpanjiang Basin mainly focused on the platform facies of the Zhuganpo Formation and Wayao Formation (Sun et al., 2016; Dal et al., 2024), primarily using biostratigraphy to constrain the timing. However, due to the complexity of Carnian conodont biostratigraphy, no consensus has been reached on a single biostratigraphic scheme (Korte et al., 2003; Orchard, 2010). Moreover, the distribution ranges of most Late Triassic conodont species are long, and the ranges of index fossils such as conodonts and ammonites have not yet met the needs for marine biostratigraphic correlation (Zhang et al., 2018). Therefore, correlation is difficult in the slope-basin zone due to the chronological framework.

The slope-basin area of the Nanpanjiang Basin develops a set of Niluo Member (NL Member) slump-folded nodular limestone, thin-bedded mudstone, and shale (Fig. 1b). Its lithology is significantly different from the turbidites of the overlying and underlying Xuman Formation (XM Formation) and Bianyang Formation (BY Formation), making it a regional marker bed. Regarding the age of the NL Member, one view considers it a marker separating the Anisian and Ladinian stages, being a synchronous heterotopic equivalent of the second Member "lacustrine-swamp layer" of the Yangliujing Formation on the platform (Guizhou Geological Survey, 2013). However, because the NL Member and BY Formation have never had absolute age reports, this age constraint is not definitive. This has led some scholars to believe that no Late Triassic marine strata have been discovered in the Nanpanjiang Basin to date (Yang et al., 2020).

This study found volcanic ash layers within the NL Member in the Wangmo area, Guizhou. This discovery consists of two sections with similar lithology (WM-a and WM-b) (Fig. 1c). Both WM-a and WM-b sections exhibit comparable freshness. Using the nodular limestone of the NL Member and the conglomerate at the base of the BY Formation as marker beds, the correlation between the two sections can be accurately constrained (Fig. 2a, 2b). In the study area, the lithology of the NL Member is consistent with that of the Ziyun-Wangmo region (edge of the slope of the Nanpanjiang Basin), characterized by dark-colored rock series. However, some thick turbiditic sandstone intercalations occur in the upper part of the NL Member. Within the NL

Member, slump folds occur in the nodular limestone, accompanied by abundant pyrite. This indicates deposition in an oxygen-deficient deep-water environment. The underlying XM Formation and overlying BY Formation both exhibit turbidites with Bouma sequences, confirming the NL Member represents a distinct segment within the several-kilometer-thick stratigraphic succession.

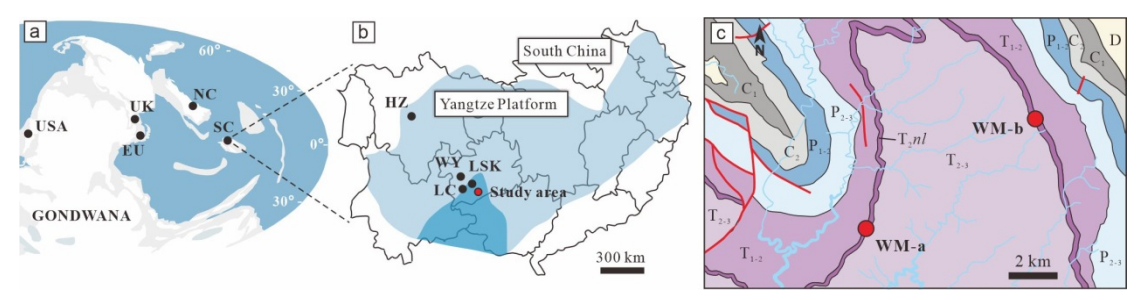


Fig. 1. Location of the study area in the Nanpanjiang Basin.

(a) Middle-Late Triassic plate configuration (modified after Scotese, 2016). SC-South China, NC-North China, UK-United Kingdom, USA-United States of America, EU-European Union; (b) Triassic palaeogeographic reconstruction of South China (modified after Sun et al., 2016). HZ-Hanzeng, WY-Wayao, LSK-Laishike, LC-Longchang; (c) Geological map of the study area.

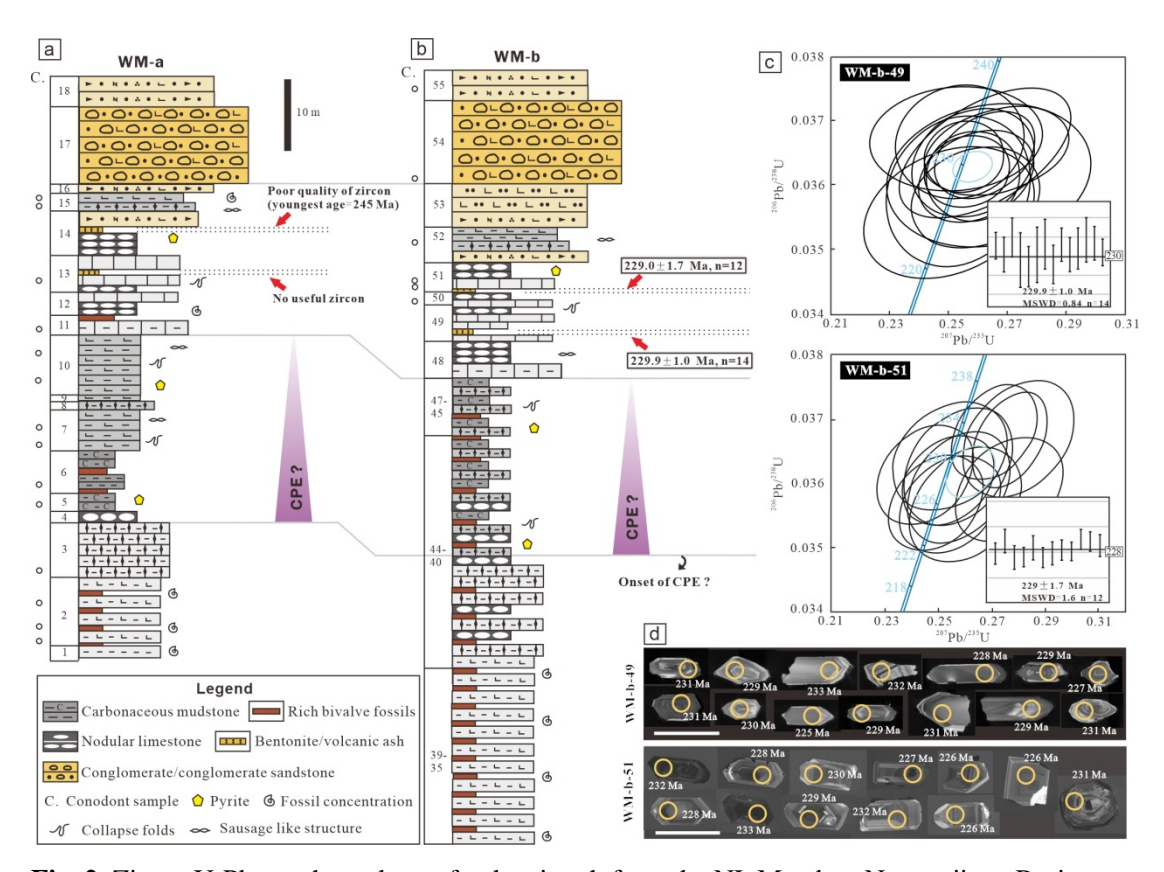


Fig. 2. Zircon U-Pb geochronology of volcanic ash from the NL Member, Nanpanjiang Basin.

scale bars in the images are 100 µm.

(a) Stratigraphic column of section WM-a; (b) Stratigraphic column of section WM-b; (c) Concordia plots and weighted mean ages for zircons from volcanic ash WM-b-49 and WM-b-51; (d) Representative cathodoluminescence images of zircons from the two volcanic ash layers. The

Both sections developed two layers of volcanic ash (Supplementary Materials Fig. S1). To avoid accidental errors, we sampled twice and sent the samples to Nanjing Hongchuang Exploration Technology Service Co., Ltd and Wuhan Sample Solution Analytical Technology Co., Ltd. for U-Pb dating of zircons respectively (Supplementary Materials Table. S1, Table S2). The results show that the volcanic ash in WM-a section (layers 13 and 14) contained few zircons, mostly fragmented, with the youngest single zircon age at 245 Ma. The zircons from the two volcanic ash layers in the WM-b section were more complete with clear zoning. This indicates that these zircons are of magmatic origin. Layer 49 yielded a weighted age of 229.9±1.0 Ma (MSWD=0.84) (Fig. 2c, 2d), with an average zircon Th/U ratio of 0.417. Layer 51 yielded a weighted age of 229.0±1.7 Ma (MSWD=1.6) (Fig. 2c, 2d), with an average zircon Th/U ratio of 0.775. Both volcanic ash layers indicate that the NL Member is within the Carnian Stage. This age is much younger than the previously suggested depositional time of the NL Member (Anisian/Ladinian boundary, ~241.46 Ma).

In this study, conodont fossil samples were concurrently collected from both sections (sampling locations shown in Fig. 2a, 2b). Unfortunately, none of the 41 conodont samples yielded age-diagnostic fossils. The primary reason may be that prolonged and intense turbiditic environments were unsuitable for conodont survival. Additionally, according to zircon U-Pb dating results, conodont diversity and distribution during this period (Carnian) were far less abundant than in the early Triassic (the results of conodont fossils will be published later). This further validates the difficulty in correlating deep-water and shallow-water chronostratigraphic frameworks using conodonts.

Compared to turbidites, the NL Member represents slow sedimentation (or starved sedimentation). In the deep-water area of the Nanpanjiang Basin, the turbidite sedimentary thickness is enormous: the XM Formation is >2700 m, and the BY Formation is ~2120 m (Guizhou Geological Survey, 2013). Although the Triassic was a time of frequent volcanic activity, turbidite sedimentation—due to ample sediment supply—could easily dilute any coeval volcanic ash, making it difficult to preserve. Therefore, the volcanic ash within the NL Member is valuable chronological material. Whereas the upper part of the NL Member contains turbidite interlayers, we estimate that its base is ~234 Ma based on the proportion of slow sedimentation (Supplementary Materials Fig. S2), which coincides with the known initiation age range of the CPE. In shallow water systems, the input of terrigenous clastics or volcaniclastic material is one of the important factors for the demise of platform carbonates (Lehrmann et al., 1998; Wilson and Lokier, 2002). When terrigenous siliciclastic input accelerates into the near-shore basin, suspended matter increases water turbidity, reduces photic zone thickness, inhibits primary productivity, and causes the migration or disappearance of main carbonate deposition (Bodin et al., 2017; Shi et al., 2017). Therefore, the carbonate retreat caused by the CPE might preserve evidence in slope facies environments. The NL Member is distinctly different from the sandstone, siltstone, and shale assemblages in the overlying and underlying strata. It is the only carbonate deposit in the regional slope-basin zones. Moreover, evidence indicates that sedimentation rates increased in the western Tethys during the CPE, while the opposite trend occurred in the eastern Tethys (Dal et al., 2024). Lithofacially, the NL Member matches this characteristic. Therefore, this suite of features suggests that the Niluo Member may record the CPE. These age data serve as a new anchor point for Late Triassic stratigraphic correlation in South China and show potential for correlating CPE sediments.

Conflict of interest

The author declares that no conflict of interest.

Acknowledgments

This work was supported by the National Natural Science Foundation of China [grant number 42001011]; the Fundamental Research Funds for Central Public Welfare Research Institutes, CAGS [grant number JKYQN202365]; the Guangxi Natural Science Foundation [grant number 2022GXNSFBA035592]; the China Geological Survey [grant number DD20221637].

Corresponding author

E-mail address: wuliangjun@mail.cgs.gov.cn (L. Wu).

References

- [1] Sun, Y. D., Wignall, P. B., Joachimski, M. M., et al., 2016. Climate warming, euxinia and carbon isotope perturbations during the Carnian (Triassic) Crisis in South China. Earth and Planetary Science Letters 444: 88-100. http://dx.doi.org/10.1016/j.epsl.2016.03.037
- [2] Simms, M. J., Ruffell, A.H., 1989. Synchroneity of climatic change and extinctions in the Late Triassic. Geology 17: 265-268.
- [3] Klausen, T.G., Nyberg, B., Helland-Hansen, W., 2019. The largest delta plain in Earth's history. Geology 47: 470-474. https://doi.org/10.1130/G45507.1
- [4] Dal, C. J., Sun, Y. D., Kemp, D. B., 2024. Palaeogeographic heterogeneity of large-amplitude changes in marine sedimentation rates during the Carnian Pluvial Episode (Late Triassic). Earth and Planetary Science Letters 237: 104437. https://doi.org/10.1016/j.gloplacha.2024.104437
- [5] Korte, C., Kozur, H. W., Bruckschen, P., et al., 2003. Strontium isotope evolution of Late Permian and Triassic seawater. Geochimica et Cosmochimica Acta 67: 47–62. https://doi.org/10.1016/S0016-7037(02)01035-9
- [6] Orchard, M. J., 2010. Triassic conodonts and their role in stage boundary definition. In: Lucas, S.G. (Ed.). The Triassic Timescale. Geological Society, London, Special Publications 334: 139-161. https://doi.org/10.1144/SP334.7
- [7] Zhang, Z. T., Sun, Y. D., Lai, X. L., 2018. Progresses on Carnian (Late Triassic) conodont study in Southwest China. Earth Science 43: 3955-3975 (in Chinese with English Abstract). https://doi.org/10.3799/dqkx.2018.248
- [8] Guizhou Geological Survey, 2013. Regional Geology of Guizhou Province (in Chinese).
- [9] Yang, C. F., Liu, J. Z., Gu, X. X., et al., 2020. The Relationship of Tectonic Evolution and Au-Sb Mineralization in Nanpanjiang–Youjiang Basin. 41: 280-292 (in Chinese with English Abstract). https://doi.org/10.3975/cagsb.2020.021501
- [10] Lehrmann, D. J., Wei, J., Enos, P., 1998. Controls on facies architecture of a large Triassic carbonate platform: the Great Bank of Guizhou Nanpanjiang basin, South China. Journal of Sedimentary Research 68: 311-326. https://doi.org/10.2110/jsr.68.311
- [11] Wilson, M. E., Lokier, S. W., 2002. Siliciclastic and volcaniclastic influences on equatorial carbonates: insights from the Neogene of Indonesia. Sedimentology 49: 583-601. https://doi.org/10.1046/j.1365-3091.2002.00463.x

- [12] Bodin, S., Hönig, M. R., Krencker, F. N., et al., 2017. Neritic carbonate crisis during the Early Bajocian: Divergent responses to a global environmental perturbation. Palaeogeography, Palaeoclimatology, Palaeoecology 468: 184-199. https://doi.org/10.1016/j.palaeo.2016.12.017
- [13] Shi, Z. Q., Preto, N., Jiang, H. S., et al., 2017. Demise of Late Triassic sponge mounds along the northwestern margin of the Yangtze Block, South China: related to the Carnian Pluvial Phase? Palaeogeography, Palaeoclimatology, Palaeoecology 474: 247-263. https://doi.org/10.1016/j.palaeo.2016.10.031
- [14] Scotese, C. R., 2016. PALEOMAP PaleoAtlas for GPlates and the PaleoData Plotter Program. PALEOMAP Project.

Supplementary materials for

Discovery of Late Triassic volcanic ash layers in the deep-water zone of the Nanpanjiang Basin (South China) and the possibility of Carnian Pluvial Episode correlation

Liangjun Wu^{a,b,c*}

- a. Institute of Karst Geology CAGS/Key Laboratory of Karst Dynamics, MNR & GZAR/International Research Centre on Karst under the Auspices of UNESCO, 541004, Guilin, China
- b. Pingguo Guangxi, Karst Ecosystem, National Observation and Research Station, 531406, Pingguo, China
- c. College of Earth Sciences, Jilin University, 130061, Changchun, China

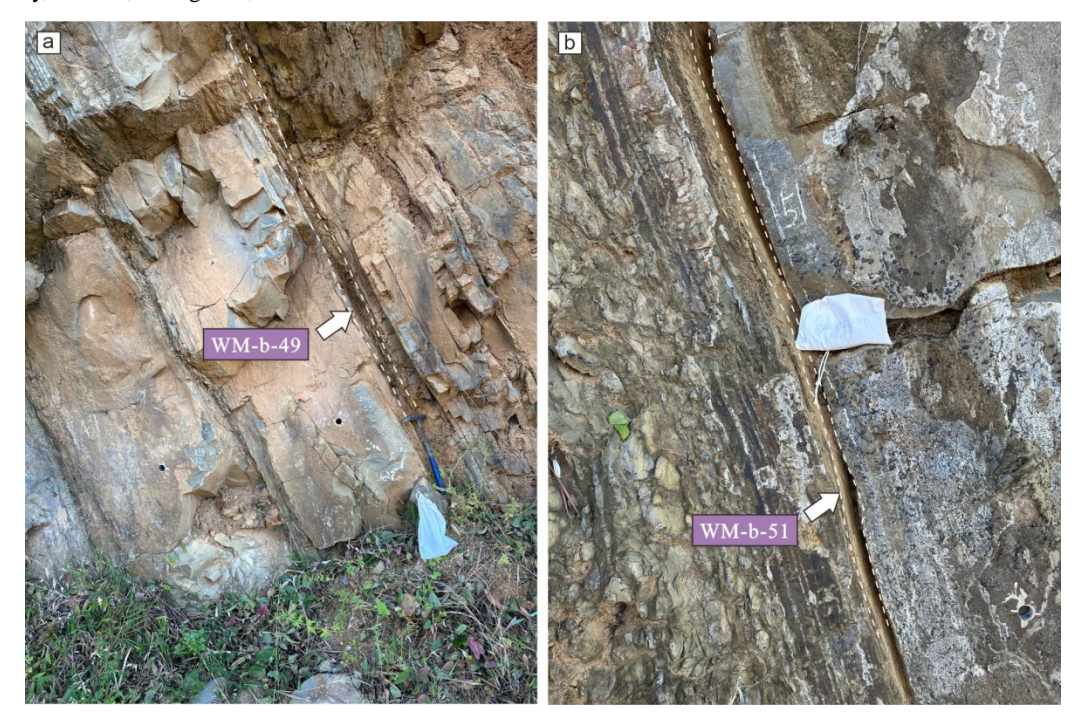


Fig. S1 The outcrop of volcanic ash layers of the WM-b section



Fig. S2 Thickness proportion of lithologies formed under rapid and slow sedimentation in the WM-b section

Note: the rapid deposition corresponds to thick-bedded calcareous siltstone and fine sandstone, while the slow deposition corresponds to dark thin-bedded mudstone, shale, and nodular limestone. Due to the wide-angle photography, the scale bar in the figure is approximate. Both the XM member (>2700 m) and BY member (~2120 m) are dominated by extremely rapid turbidite sedimentation, but their sedimentation rates decreased significantly within the CPE [1]. Turbidites occasionally develop in the NL member. Excluding the thickness of rapid deposited turbidites, the onset age of the NL member is estimated to be ~234 Ma based on the thickness of the slow deposited portion.

Table. S1 LA-ICP-MS zircon U-Pb dating data for the sample of WM-b-49

Sample	No.	Th	U	Th/U	U-Th-Pb isotope ratio							Age (Ma)					
					²⁰⁷ Pb/ ²³⁵ U		²⁰⁷ Pb.	²⁰⁷ Pb/ ²⁰⁶ Pb		²⁰⁶ Pb/ ²³⁸ U		²⁰⁷ Pb/ ²³⁵ U		²⁰⁷ Pb/ ²⁰⁶ Pb		^{/238} U	Concordance
		(ppm)	(ppm)		Ratio	2σ	Ratio	2σ	Ratio	2σ	Age	2σ	Age	2σ	Age	2σ	(%)
WM-b-49	1	217.600	11.428	0.407	0.255000	0.011000	0.050800	0.002300	0.036450	0.000450	229.9	9.2	220.0	100.0	230.8	2.8	100
	2	252.600	13.956	0.417	0.259000	0.016000	0.052500	0.003100	0.036150	0.000580	233.0	13.0	270.0	130.0	228.9	3.6	98
	3	140.200	8.091	0.412	0.252000	0.024000	0.051100	0.005200	0.036730	0.000660	231.0	21.0	170.0	200.0	232.5	4.1	99
	4	175.100	9.589	0.381	0.253000	0.020000	0.051100	0.004000	0.035920	0.000960	228.0	17.0	220.0	170.0	227.5	6.0	100
	5	170.500	10.092	0.493	0.249000	0.023000	0.050700	0.004700	0.035580	0.000830	224.0	19.0	190.0	190.0	225.4	5.2	99
	6	129.700	6.167	0.343	0.264000	0.028000	0.053200	0.005600	0.036150	0.000930	237.0	22.0	280.0	220.0	228.9	5.8	97
	7	341.200	47.391	0.049	1.720000	0.120000	0.093000	0.002500	0.133200	0.007300	1006.0	4 7.0	1479.0	53.0	805.0	42.0	78
	8	227.000	11.691	0.427	0.262000	0.024000	0.051900	0.004400	0.036510	0.000830	235.0	20.0	250.0	190.0	231.1	5.2	98
	9	297.900	16.943	0.419	0.259000	0.018000	0.052800	0.003600	0.035820	0.000640	233.0	14.0	270.0	140.0	226.9	4.0	97
	10	333.100	16.633	0.424	0.262000	0.014000	0.052200	0.002700	0.036480	0.000550	236.0	11.0	270.0	120.0	231.0	3.5	98
VV 1V1-U-47	11	181.100	10.115	0.435	0.272000	0.018000	0.056300	0.003600	0.034960	0.000740	243.0	14.0	400.0	130.0	221.5	4.6	91
	12	545.400	28.573	0.442	0.275200	0.008500	0.056300	0.001700	0.035390	0.000370	246.5	6.7	445.0	65.0	224.2	2.3	91
	13	264.600	14.370	0.479	0.258000	0.013000	0.051700	0.002700	0.036150	0.000570	232.0	11.0	240.0	120.0	228.9	3.5	99
	14	191.900	11.542	0.464	0.258000	0.017000	0.051400	0.003300	0.036360	0.000690	231.0	14.0	240.0	140.0	230.2	4.3	100
	15	302.900	15.084	0.294	0.254000	0.018000	0.050200	0.003600	0.036650	0.000730	229.0	14.0	180.0	160.0	232.0	4.6	99
	16	308.800	14.921	0.253	0.268000	0.016000	0.052100	0.003100	0.037110	0.000700	240.0	13.0	270.0	130.0	234.9	4.4	98
	17	231.700	13.114	0.481	0.309000	0.011000	0.063200	0.002100	0.035250	0.000430	272.4	8.3	675.0	72.0	223.3	2.7	80
	18	296.800	16.027	0.440	0.266000	0.020000	0.052400	0.003800	0.036540	0.000560	238.0	16.0	260.0	150.0	231.3	3.5	97
	19	802.000	43.003	0.353	0.253000	0.015000	0.051700	0.002800	0.035280	0.000620	228.0	12.0	260.0	120.0	223.5	3.9	98
	20	304.900	17.476	0.429	0.256000	0.012000	0.051500	0.002500	0.036220	0.000450	233.0	10.0	230.0	100.0	229.4	2.8	98

Brief description of experimental methods and equipments:

The U-Pb dating of sample WM-b-49 was conducted using LA-ICP-MS in Nanjing Hongchuang Exploration Technology Service Co., Ltd. The Resolution SE model laser ablation system (Applied Spectra, USA) was equipped with ATL (ATLEX 300) excimer laser and a Two Volume S155 ablation cell. The laser ablation system was coupled to an Agilent, USA).

Detailed tuning parameters can be seen in [2]. LA-ICP-MS tuning was performed using a 50 micron diameter line scan at 3 μ m/s on NIST 612 at ~3.5 J/cm² with repetition rate 10 Hz. Adjusting the gas flow to get the highest sensitivity (238 U~6*10⁵ cps) and the lowest oxide ratio(ThO/Th<0.2%). P/A calibration was conducted on the NIST 610 using a 100 micron diameter line scan. Other laser parameters are the same as that of tuning. Mass analyzed were 29 Si , 31 P, 45 Sc, 49 Ti, 56 Fe, 89 Y, 91 Zr, 93 Nb, 139 La, 140 Ce, 141 Pr, 146 Nd, 147 Sm, 151 Eu, 157 Gd, 159 Tb, 163 Dy, 165 Ho, 166 Er, 169 Tm, 173 Yb, 175 Lu, 178 Hf, 181 Ta, 202 Hg, 204 Pb, 206 Pb, 207 Pb, 208 Pb, 232 Th, 235 U and 238 U, with a total sweep time of ~ 0.23 seconds. Zircon were mounted in epoxy discs, polished to expose the grains, cleaned ultrasonically in ultrapure water, then cleaned again prior to the analysis using AR grade methanol. Pre-ablation was conducted for each spot analysis using 5 laser shots (~0.3 μ m in depth) to remove potential surface contamination. The analysis was performed using 30 μ m diameter spot at 5 Hz with fluence of 2.5 J/cm².

Iolite software package was used for data reduction [3]. Zircon 91500 and GJ-1 was used as primary and secondary reference materials respectively. Triplets of 91500 and GJ-1 were bracketed between multiple groups of 10 to 12 sample unknowns. Typically, 35-40 seconds of the sample signals were acquired after 20 seconds gas background measurement. Using the exponential function to calibrate the downhole fractionation [3]. Iolite software package ('3D Trace Element') was used for data reduction [4]. Measured ages of 91500 (1061.5±3.2 Ma, 2σ) and GJ-1 (601.7±4.2 Ma, 2σ) are well within 1% of the accepted age.

Table. S2 LA-ICP-MS zircon U-Pb dating data for the sample of WM-b-51

Sample	No.	Th	U	Th/U	U-Th-Pb isotope ratio							Concordonos					
					²⁰⁷ Pb/ ²³⁵ U		²⁰⁷ Pb	$^{207}\text{Pb}/^{206}\text{Pb}$		206 Pb/ 238 U		$^{207}\text{Pb}/^{235}\text{U}$		²⁰⁷ Pb/ ²⁰⁶ Pb		Pb/ ²³⁸ U	Concordance
		(ppm)	(ppm)		Ratio	1σ	Ratio	1σ	Ratio	1σ	Age	1σ	Age	1σ	Age	1σ	(%)
WM-b-51	1	510	817	0.624207	0.2762	0.0083	0.0558	0.0018	0.0359	0.0003	248	6.575356	456	72.215	227	2.081509	91%
	2	266	399	0.665966	0.2799	0.0085	0.0549	0.0016	0.0367	0.0004	251	6.758405	409	64.8075	232	2.322192	92%
	3	291	355	0.817975	0.2600	0.0085	0.0528	0.0017	0.0357	0.0004	235	6.854783	320	74.065	226	2.301401	96%
	4	900	714	1.260387	0.2490	0.0071	0.0506	0.0015	0.0357	0.0003	226	5.813204	233	73.135	226	1.916309	99%
	5	254	381	0.666067	0.2573	0.0082	0.0515	0.0016	0.0363	0.0004	233	6.663885	261	72.21	230	2.360897	98%
	6	506	541	0.936755	0.2543	0.0077	0.0517	0.0016	0.0357	0.0003	230	6.218855	272	63.88	226	1.939243	98%
	7	369	541	0.681211	0.2575	0.0078	0.0519	0.0015	0.0359	0.0004	233	6.319014	280	68.51	228	2.233965	97%
	8	583	566	1.02854	0.2450	0.0074	0.0492	0.0015	0.0361	0.0003	223	5.999597	167	74.9875	229	1.980645	97%
	9	595	551	1.079971	0.2535	0.0070	0.0508	0.0014	0.0361	0.0003	229	5.707914	232	62.9525	228	1.798445	99%
	10	708	1244	0.569391	0.2709	0.0065	0.0531	0.0012	0.0368	0.0003	243	5.194293	345	53.7	233	1.906205	95%
	11	299	1765	0.169653	0.2766	0.0058	0.0546	0.0012	0.0367	0.0003	248	4.581595	394	54.625	232	1.897308	93%
	12	395	493	0.801565	0.2542	0.0087	0.0505	0.0018	0.0364	0.0003	230	7.075693	217	49.0675	231	2.16445	99%
	13	242	198	0.624207	0.5782	0.0196	0.0641	0.0023	0.0654	0.0006	463	12.63066	746	41.6625	409	3.381966	87%
	14	1046	760	0.665966	0.3060	0.0082	0.0606	0.0015	0.0364	0.0003	271	6.374801	626	55.545	231	1.858798	83%

Brief description of experimental methods and equipments:

This sample WM-b-51, the U-Pb dating and trace element analysis of zircon were simultaneously conducted by LA-ICP-MS at the Wuhan SampleSolution Analytical Technology Co., Ltd., Wuhan, China. Detailed operating conditions for the laser ablation system and the ICP-MS instrument and data reduction are the same as description by [5]. Laser sampling was performed using a GeolasPro laser ablation system that consists of a COMPexPro 102 ArF excimer laser (wavelength of 193 nm and maximum energy of 200 mJ) and a MicroLas optical system. An Agilent 7700e ICP-MS instrument was used to acquire ion-signal intensities. Helium was applied as a carrier gas. Argon was used as the make-up gas and mixed with the carrier gas via a T-connector before entering the ICP. A "wire" signal smoothing device is included in this laser ablation system [6]. The spot size and frequency of the laser were set to xxµm and xxHz, respectively, in this study. Zircon 91500 and glass NIST610 were used as external standards for U-Pb dating and trace element calibration, respectively. Each analysis incorporated a background acquisition of approximately 20-30 s followed by 50 s of data acquisition from the sample. An Excel-based software ICPMSDataCal was used to perform off-line selection and integration of background and analyzed signals, time-drift correction and quantitative calibration for trace element analysis and U-Pb dating [7,8]. Concordia diagrams and weighted mean calculations were made using Isoplot/Ex_ver3 [9].

Reference

- [1] Dal, C.J., Sun, Y.D., Kemp, D.B., 2024. Palaeogeographic heterogeneity of large-amplitude changes in marine sedimentation rates during the Carnian Pluvial Episode (Late Triassic). Earth and Planetary Science Letters 237: 104437. https://doi.org/10.1016/j.gloplacha.2024.104437
- [2] Hu, Z.C., Zhang, W., Liu, Y.S., et al., 2015. "Wave" signal-smoothing and mercury-removing device for laser ablation quadrupole and multiple collector ICPMS analysis. Analytical Chemistry 87: 1152–1157. https://doi.org/10.1021/ac503749k
- [3] Liu, Y.S., Gao, S., Hu, Z.C., et al., 2010. Continental and oceanic crust recycling-induced melt-peridotite interactions in the Trans-North China Orogen. Journal of Petrology 51: 537–571. https://doi.org/10.1093/petrology/egp082
- [4] Liu, Y.S., Hu, Z.C., Gao, S., et al., 2008. In situ analysis of major and trace elements of anhydrous minerals by LA-ICP-MS without applying an internal standard. Chemical Geology 257: 34-43. https://doi.org/10.1016/j.chemgeo.2008.08.004
- [5] Ludwig, K.R., 2003. ISOPLOT 3.00: A Geochronological Toolkit for Microsoft Excel. Berkeley Geochronology Center.
- [6] Paton, C., Woodhead, J.D., Hellstrom, J.C., et al., 2010. Improved laser ablation U-Pb zircon geochronology through robust downhole fractionation correction. Geochemistry, Geophysics, Geosystems 11: Q0AA06. https://doi.org/10.1029/2009GC002618
- [7] Paul, B., Petrus, J., Savard, D., et al., 2023. Time resolved trace element calibration strategies for LA-ICP-MS. Journal of Analytical Atomic Spectrometry. https://doi.org/10.1039/d3ja00037k
- [8] Thompson, J., Meffre, S., Danyushevsky, L., 2018. Impact of air, laser pulse width and fluence on U-Pb dating of zircons by LA-ICPMS. Journal of Analytical Atomic Spectrometry 33: 221-230. https://doi.org/10.1039/C7JA00357A
- [9] Zong, K.Q., Klemd, R., Yuan, Y., et al., 2017. The assembly of Rodinia: The correlation of early Neoproterozoic (ca. 900 Ma) high-grade metamorphism and continental arc formation in the southern Beishan Orogen. Precambrian Research 290:

32–48. https://doi.org/10.1016/j.precamres.2016.12.010